



HAL
open science

Imidazolium-based poly(ionic liquid)/ionic liquid solutions: Rheology, structuration and ionic transport properties

Biao Zhang, Guillaume Sudre, Guilhem Quintard, Anatoli Serghei, Julien Bernard, Etienne Fleury, Aurélia Charlot

► **To cite this version:**

Biao Zhang, Guillaume Sudre, Guilhem Quintard, Anatoli Serghei, Julien Bernard, et al.. Imidazolium-based poly(ionic liquid)/ionic liquid solutions: Rheology, structuration and ionic transport properties. *Polymer*, 2021, 237, pp.124305. 10.1016/j.polymer.2021.124305 . hal-03412987

HAL Id: hal-03412987

<https://hal.science/hal-03412987>

Submitted on 3 Nov 2021

HAL is a multi-disciplinary open access archive for the deposit and dissemination of scientific research documents, whether they are published or not. The documents may come from teaching and research institutions in France or abroad, or from public or private research centers.

L'archive ouverte pluridisciplinaire **HAL**, est destinée au dépôt et à la diffusion de documents scientifiques de niveau recherche, publiés ou non, émanant des établissements d'enseignement et de recherche français ou étrangers, des laboratoires publics ou privés.

Imidazolium-based poly(ionic liquid)/ionic liquid solutions: rheology, structuration and ionic transport properties

Biao Zhang,^{a,b*} Guillaume Sudre,^c Guilhem Quintard,^b Anatoli Serghei,^c
Julien Bernard,^b Etienne Fleury,^{b*} Aurélie Charlot^{b*}

^a *Frontiers Science Center for Flexible Electronics (FSCFE), Xi'an Institute of Flexible Electronics (IFE) and Xi'an Institute of Biomedical Materials & Engineering (IBME), Northwestern Polytechnical University (NPU), Xi'an, 710072 Shaanxi, China*

^b *Université de Lyon, INSA Lyon, CNRS IMP 5223, 69621 Villeurbanne Cedex, France.*

^c *Université de Lyon, Université Lyon 1, CNRS IMP5223, 15 Bd. A. Latarjet, 69622 Villeurbanne Cedex, France.*

Fax: +33 (0)4 72 43 85 27; Tel: +33 (0)4 72 43 63 38; E-mail, etienne.fleury@insa-lyon.fr,
aurelia.charlot@insa-lyon.fr, iambzhang@nwpu.edu.cn

Abstract

RAFT-made poly(ionic liquid) chains (PIL), poly(1-[2-acryloylethyl]-3-methylimidazolium bromide) (Poly [AEmim][Br]), have been mixed with a ionic liquid (IL), namely butylmethylimidazolium chloride ([C4mim][Cl].) The similarities in terms of structure and polarity of these molecular and macromolecular imidazolium derivatives led to homogeneous and transparent solutions. The influence of the chain molar mass and the concentration was examined through rheology investigation. It was established that the steady-shear viscosity of the solutions, and the viscoelastic properties can be finely tuned by these two parameters and by temperature. The thermal-dependence of the rheological features allowed for determining

high activation energies (E_a) (around 80 kJ/mol), compared to analogous PIL aqueous solutions. Such E_a values reflect high cohesion in PIL/IL solutions, related to the formation of multiple strong interactions, such as hydrogen bonds, van der Waals forces and Coulomb interactions between ionic species. Wide-angle and small-angle X-ray scattering experiments as well as scanning electron microscopy analysis evidenced a multi-scale local homogeneity of the PIL/IL solutions, which additionally exhibit high ionic conductivity (*ca.* 10^{-3} S/cm at 30 °C), as measured by broadband dielectric spectroscopy.

Key words. ionic liquid, poly(ionic liquid), rheology

1. Introduction

Ionic liquids (ILs) are a peculiar class of salts with a melting point lower than 100 °C. These molecular species display a set of properties, such as non-flammability and low vapor pressure, high thermal and chemical stability, exceptional ionic conductivity [1-5]. As innovative fluids, ILs have received great attention in chemistry, materials science, chemical engineering, and environmental science during the past two decades [6]. Moreover, IL molecules can be found as monomers (vinyl, acrylate, etc.) that can be polymerized by conventional or controlled radical polymerization (CRP) to generate poly(ionic liquid)s (PILs) [7-16]. PILs constitute an original and promising family of polyelectrolytes combining exceptional features emanating from ionic liquids with the properties of polymer materials, in terms of mechanical reinforcement, easy processability and possibility to tune the properties by the macromolecular engineering [17]. However, compared to pure ILs, PILs often suffer from the relatively lower conductivity owing to the limited mobility of the ionic backbone since only counter-anions behave as mobile charge carriers. In order to enhance the ionic conductivity of PIL macromolecules, their association with ILs appeared as a promising way

and the resulting ionic binary mixtures have been employed as quasi-solid electrolytes [18-20]. For example, Cowan *et al.* developed a hydrophobic imidazolium-based PIL/IL ionogel, exhibiting ionic conductivity values $\geq 10^{-2}$ S/cm at 25 °C and $\approx 10^{-1}$ S/cm at 110 °C, respectively [18]. De Oliveira *et al.* prepared PIL/IL electrolytes by mixing a PIL matrix with two different ILs (*i.e.* 1-methyl-3-butylimidazolium bis(fluorosulfonyl)imide and 1,2-dimethyl-3-propylimidazolium bis(trifluoromethylsulfonyl)imide) [20]. The resulting hydrophobic gel electrolytes could be used as supercapacitors, since they displayed a conductivity of 3.2×10^{-3} S/cm and 5.0×10^{-4} S/cm with electrochemical windows of 2.8 V and 3.0 V, respectively. Zhao *et al.* dissolved poly(1-butyl-3-vinylimidazolium bromide) ([PBVIm][Br]) and poly(1-butyl-3-vinylimidazolium bis(trifluoromethanesulfonyl)imide) ([PBVIm][TFSI]) in a mixture of 1-propyl-3-methylimidazolium iodide (PMII) /1-ethyl-3-methylimidazolium bis((trifluoromethyl)sulfonyl)imide (EMITFSI) to fabricate quasi-solid-state dye-sensitized solar cells (DSSCs) [21]. The electrolytes displayed a conductivity of 3.2×10^{-3} S/cm with an electrochemical window of 2.8 V. The resulting cells were shown to exhibit superior long-term stability due to their non-volatile character.

PIL/IL composites have also been prepared as membranes for gas separation [22]. Due to the attributes linked to the mechanical stability of PIL and the high gas permeability and diffusivity of IL molecules, PIL/IL membranes have been utilized for the separation of CO₂/N₂, CO₂/CH₄, CO₂/H₂ etc. [23-31]. More recently, Sappidi *et al.* studied mixtures composed of ionenes of varied structures (cationic imidazolium polymers formed from condensation reactions) in 1-ethyl-3-methylimidazolium bistriflimide [32]. The authors investigated the interactions using molecular dynamics simulations. They demonstrated that the structure of the ionenes (more or less flexible) strongly impact both the interactions developed within the mixtures and the conformation adopted by the chain in IL medium.

In summary, the literature emphasizes that PIL/IL mixtures have mainly been explored for

specific applications, without a full understanding of their physico-chemical behavior. Moreover, the existing literature demonstrates that most of works have been devoted to mixtures including hydrophobic IL derivatives, with nearly no study dealing with hydrophilic species including halide anions. Herein, we present a thorough physico-chemical scrutiny of binary PIL/IL systems resulting from the simple addition of precisely-defined poly(1-[2-acryloylethyl]-3-methylimidazolium bromide) chains (poly [AEmim][Br]) (synthesized by RAFT polymerizations) into 1-butyl-3-methylimidazolium chloride ([C4mim][Cl]), both being fully hydrophilic and compatible imidazolium-based IL derivatives. Halide-anion based PIL/IL mixtures are polar mixtures, in which the chloride and bromide anions can be easily engaged into the formation of hydrogen bonds which are known to enhance the cohesion of a given ionic liquid-based mixture. In this work, we are specifically interested in the rheological properties of (poly [AEmim][Br]) /([C4mim][Cl]) mixtures with a focus on the impact of the PIL molar mass and concentration, and temperature. Steady-shear viscosity and viscoelastic properties of the mixtures are studied and the energies of activation are determined and compared to PIL/water systems. The internal morphology and the ionic transport properties of the binary mixtures are further examined by small and wide-angle X-ray scattering, scanning electron microscopy and broadband dielectric spectroscopy, respectively.

2. Experimental Section

2.1 Materials

1-butyl-3-methylimidazolium chloride ([C4mim][Cl]) (> 97 %, mp 75 °C) was purchased from Sigma-Aldrich and will be denoted as IL (for ionic liquid) in the following of the manuscript. S-ethyl-S'-(α,α' -dimethyl- α'' -acetic acid)trithiocarbonate (EMP) was used as chain transfer agent (CTA).

2.2 PIL/IL mixture preparation

Synthesis of PIL: The synthesis of the imidazolium acrylate-based ionic liquid (1-[2-acryloylethyl]-3-methylimidazolium bromide: [AEmim][Br]) as well as its RAFT polymerization have been described elsewhere [33,34]. The notations PIL_{10K}, PIL_{25K} and PIL_{100K} correspond to (poly [AEmim][Br]) having a theoretical molar mass ($M_{n,theo}$) close to 10, 25 and 100 kg/mol, respectively. Conditions of RAFT polymerization and structural characteristics of the resulting PILs are gathered in Table S1. ¹H NMR spectra and size exclusion chromatography (SEC) of the PILs are given in Fig. S1 and S2. The true molar masses for PIL_{10K} and PIL_{25K} were determined by ¹H NMR spectroscopy from the relative integration of signals attributed to the chain end group and polymer backbone. From SEC analyses (obtained after anion exchange, and analyzed in DMF/LiTfSI, PS standards), [32,33] all PILs present a unimodal, narrow molar mass distribution ($\mathcal{D} < 1.30$) (Fig. S2). PIL and IL were carefully dried at 80 °C under vacuum overnight before any use.

Typical procedure for the preparation of a PIL/IL mixture: An appropriate mass of dried PIL (PIL_{10K}, PIL_{25K} or PIL_{100K}) was added to dried IL under magnetic stirring for 12 h under argon at 80 °C. Mass fractions (wt. %) of PIL were varied depending on the analysis to be performed. The resulting samples were macroscopically transparent. They were stored under dry N₂ atmosphere to avoid water uptake. In the following of this article, the sample nomenclature will be further defined as PIL_x (y %)/IL, where x corresponds to the M_n of the PIL, and y stands for the mass fraction of PIL, respectively.

2.3 Characterization

Rheological measurements. The shear viscosity (η) of all samples was measured by using a controlled-stress rheometer (DHR2, TA Instruments Inc., UK) with an aluminum plate geometry (diameter 40 mm, gap 500 μ m). The overlap concentration (C^*) was determined

from the logarithmic evolution of viscosity (η) at the Newtonian plateau ($\eta_{Newtonian}$) (at 1 s^{-1}) as a function of the PIL concentration. C^* was considered as the concentration for which $\eta_{Newtonian}$ locates at the crossover between the two viscosity regimes characterized by different power laws [35-37]. Dynamic rheological measurements in oscillation mode were checked as a function of strain amplitude to ensure data were collected in the linear domain. Typically, during the dynamical measurements, the applied strain was settled at 1 % for the PIL/IL mixtures. The temperature was precisely controlled by a Peltier system. A classical aluminium cover in inert metal, placed on the top of the superior plate of the rheometer, was used to perform the analysis under controlled atmosphere and to prevent water uptake. The rheological properties were proven to be reproducible and stable on the time scale of the experiment (Fig. S3).

Thermogravimetric analysis. TGA measurements were performed under nitrogen using a TA Instruments TGA Q500 apparatus. Samples of about 10 mg were heated from $30 \text{ }^\circ\text{C}$ to $550 \text{ }^\circ\text{C}$ at a heating rate of $10 \text{ }^\circ\text{C}/\text{min}$.

Differential scanning calorimetry. DSC measurements were conducted under nitrogen atmosphere using a TA Instruments (model Q10, USA) at a heating/cooling rate of $10 \text{ }^\circ\text{C}/\text{min}$. Two cycles (heating-cooling-heating) were performed for each sample from $-70 \text{ }^\circ\text{C}$ to $200 \text{ }^\circ\text{C}$. The glass transition temperature (T_g) values of PIL_{10K}, PIL_{25K} and PIL_{100K} were determined during the second heating cycle, where the midpoint of the thermal transition was considered. The T_g values of PIL_{10K}, PIL_{25K} and PIL_{100K} are 39, 54 and $65 \text{ }^\circ\text{C}$, respectively (Fig. S4).

Cryo-SEM analysis. The sample was inserted in a sample holder at room temperature, delicately introduced in a Gatan Alto 2500 cryo-chamber and slowly cooled down to $-150 \text{ }^\circ\text{C}$. Then, it was fractured with a cold blade and a platinum coating was applied to increase the surface conductivity. The sample was then introduced into the microscope chamber where the temperature was maintained at $-150 \text{ }^\circ\text{C}$ during the analysis. Samples were observed on a FEI

Quanta 250 scanning electron microscope at an accelerating voltage of 10 kV. The energy-dispersive X-ray (EDX) spectroscopy analysis was collected on various $5\ \mu\text{m} \times 5\ \mu\text{m}$ zones at $-150\ \text{°C}$.

X-ray scattering Analysis. Small and wide-angle X-ray scattering (SAXS and WAXS) measurements were conducted at the European Synchrotron Radiation Facility (ESRF, Grenoble, France) on BM02-D2AM beamline. After drying at $80\ \text{°C}$ under vacuum for one night, IL or PIL/IL samples were transferred to capped glass capillaries with internal diameter of 2.6 mm and wall thickness of 0.2 mm (Deutero GMBH, 29604 15). All samples were equilibrated at $25\ \text{°C}$ before measurements. The incident photon energy E was set at 17.000 keV. The sample-to-detector (D) distances were set to 1.57 m and ≈ 10 cm for SAXS and WAXS measurements, leading to a q -range from 1×10^{-2} to $2.3 \times 10^{-1}\ \text{Å}^{-1}$ in the SAXS configuration and from 0.22 to $3\ \text{Å}^{-1}$ in the WAXS configuration, respectively. Attenuators were used to determine the position of the direct beam and a silver behenate standard was used for calibration. After correction, the resulting two-dimensional data were averaged azimuthally to get intensity vs scattering vector q ($q = (4\pi/\lambda) \sin(\theta)$, where 2θ represents the scattering angle and λ represents the incident wavelength). After correction of the scattering from the empty glass capillaries, the scattering data were normalized according to the attenuation and thickness of the samples. For data treatment, as the bromide from brominated PIL (poly[AEmim][Br]) can be exchanged with chloride from IL (*i.e.* [C4mim][Cl]), the solvent contribution cannot be subtracted.

Ionic conductivity measurements. Ionic conductivity was measured using a high-resolution Alpha-Analyzer (Novocontrol GmbH) assisted by a Quatro temperature controller. The samples were prepared by placing the material under study between two freshly polished platinum electrodes. The thickness of the sample cell was controlled by employing 1 mm thick Teflon spacers. Frequency sweeps were isothermally performed from 10 MHz to 0.1 Hz

by applying a sinusoidal voltage of 0.1 V over a range of temperature from 30 °C to - 60 °C or from 140 °C to - 60 °C in steps of 10 °C. The ionic conductivity of the materials under investigation, corresponding to direct current conductivity (σ_{DC}) of the samples, is determined by definition from the value of the plateau observed in the frequency dependence of σ' . The plateau corresponds to the spectral region where the electrical response is dominated by the long-range diffusion of the ionic species [38,39]. The measurements were carried-out before and after thermal treatments performed in the cryostat of the dielectric spectrometer under a flow of pure nitrogen. The optimal drying step consisted in a thermal treatment of 6 h at 140 °C under nitrogen flow, thus excluding the presence of oxygen and humidity in the measurement chamber. After completing the measurements, the conductivity values were re-measured to ensure stable and reproducible experimental results. The reproducibility was additionally verified by measuring conductive properties on two different samples made of the same components with similar compositions.

3. Results and discussion

Incorporation of poly([AEmim][Br]) in dried [C4mim][Cl] leads to the formation of transparent and macroscopically homogeneous solutions, as shown in Fig. 1. The macroscopic homogeneity of the solutions can be ascribed to the good solvating/dissolution capability of [C4mim][Cl] for these PIL chains, whatever the molar mass and the concentration of PILs. Poly([AEmim][Br]) and [C4mim][Cl] present strong similarities in terms of chemical structure and polar character, allowing for the promotion and the development of strong and multiple interactions. Indeed, PIL and IL are able to interact with each other through *i*) hydrogen bonds, *ii*) Van der Waals forces, and *iii*) Coulomb interactions between cations and anions. It is important to mention that contrary to pure [C4mim][Cl] which (slowly) recrystallizes with time once molten, the PIL/[C4mim][Cl] solutions at 25 °C present an outstanding long-lasting macroscopic stability (whatever the M_n of PIL and up to 20 wt. %),

without noticeable demixion or (re)solidification. This stability with time is due to the PIL/IL favorable interactions, which prevent any recrystallization phenomena.

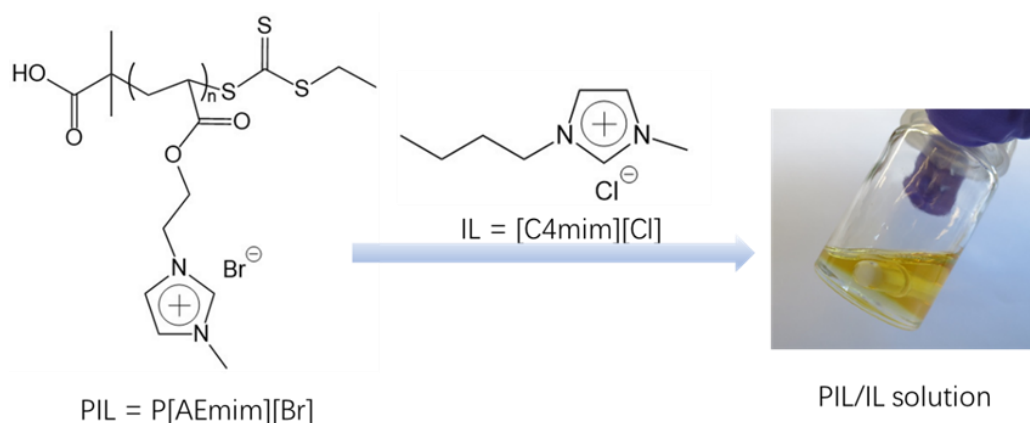


Fig. 1. Route to PIL/IL solutions. The insert photo corresponds to PIL100K at 10 wt. % in [C4mim][Cl].

3.1. Rheological investigation of PIL/IL solutions

3.1.1. Steady-shear viscosity of PIL/IL solutions

The rheological behaviors of PIL/IL solutions were examined. Despite the relatively widespread works dealing with the synthesis of PIL chains, the study of their behavior in IL medium has rarely been reported so far in the literature [13,22]. Srouf *et al.* investigated the rheological properties of hydrophobic imidazolium and pyrrolidinium-based PIL/IL ionogels.[13] The authors reported the effect of the nature of the cation on the mechanical behavior. The evolution of viscosity with the shear rate were investigated in-depth for the three PILs (PIL_{10K}, PIL_{25K} and PIL_{100K}) dissolved at various concentrations in [C4mim][Cl] (from 0.1 to 50 wt. % for PIL_{10K}, from 0.1 to 30 wt. % for PIL_{25K} and from 0.1 to 20 wt. % for PIL_{100K}). The shear viscosity of pure [C4mim][Cl] exhibits a Newtonian behavior with a viscosity of 3.65 Pa.s (Fig. S5). An illustration for the PIL_{10K}/[C4mim][Cl] binary system is provided in Fig. 2. As expected, the steady shear viscosity increases with the PIL concentration; a Newtonian plateau is observed for the whole shear rate range, except for the highest concentrations (at 40 and 50 wt. %), for which a slight shear-thinning behavior appears. The shear-thinning feature is significantly more pronounced when the PIL molar

mass increases. As shown in Fig. S6 and S7, the shear-thinning features start from the concentrations of $\sim 5\%$ and $\sim 0.5\%$ for PII_{25K}/IL and PII_{100K}/IL, respectively.

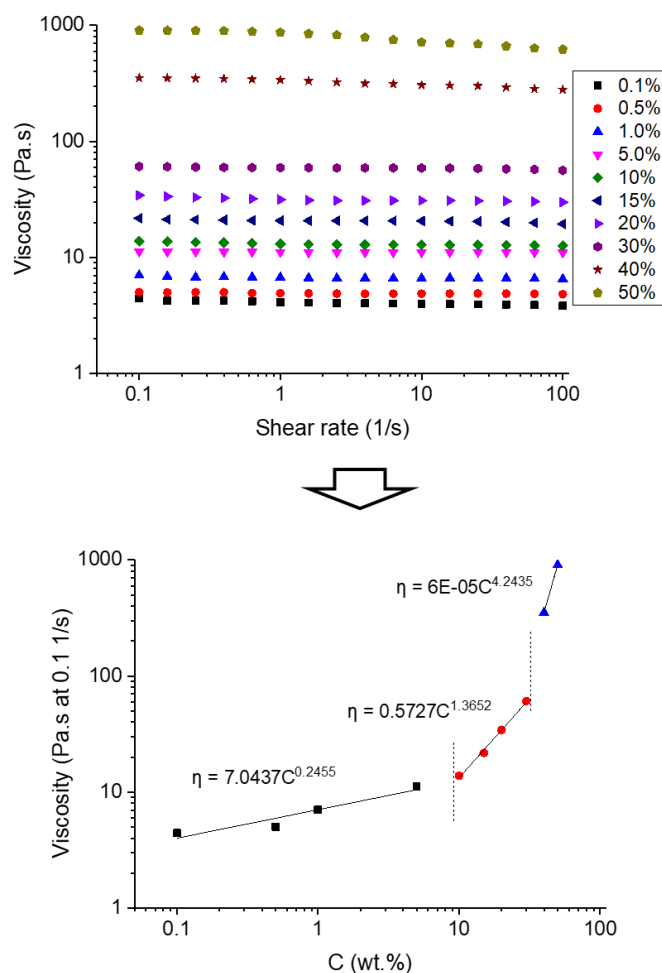


Fig. 2 (Up) Evolution of viscosity, as a function of shear rate, for PII_{10K}/IL solutions at different mass concentrations; (Down) Concentration-dependence of zero shear viscosity.

The concentration-dependence of the zero-shear viscosity (η_0 , *i.e.* viscosity considered at a rate of 0.1 s^{-1}) was monitored for each PIL/IL combination, in order to determine the overlap concentration (C^*) of PIL chains in the [C4mim][Cl] medium (Fig. 2, Down). This critical concentration is commonly considered as the concentration for which the volume of the solvated polymer chains equals the volume of the whole solution and corresponds to the concentration delimiting the dilute regime and the semi-dilute regime. In general, whereas a

linear dependence is observed in the dilute regime, higher power laws with $\eta \sim C^n$ (n around 5/4) characterize the unentangled semi-dilute regime [40,41]. The classical existing molecular interpretations developed for common polyelectrolytes [42] in saline medium and for neutral polymers [43,44] are applied to polymer chains solubilized in low viscosity solvent. Herein, the study focuses on a singular class of flexible polyelectrolyte developing strong polar interactions (and anion exchange) with an organized and highly viscous solvent ([C4mim][Cl]) [45]. Consequently, the theoretical predictions do not apply to our experimental data, which is why no linear evolution (with $n=1$) is observed. However, for the three PIL molar masses, a first domain for which η_0 slightly varies with the PIL concentration is observed at low concentrations (typically n around 0.2, Fig. 2), followed by a much more noticeable η_0 -concentration dependence (power law of 1.36). This change of slope can be the result of the transition from the dilute to the semi-dilute regime, and the corresponding critical concentration can be defined as the overlap concentration. Some connections between the polymer chains begin to occur. From $C = 40$ % wt, a higher slope (around 4.2) is observed, typical of the semi-dilute entangled regime: this strong variation can be ascribed to the presence of numerous chain entanglements which govern the viscosity behavior. Thus, it results that the C^* of PIL_{10K}, PIL_{25K} and PIL_{100K} in [C4mim][Cl] is around 9.4, 3.5 and 0.5 wt. %, respectively. As expected, C^* considerably decreases with the PIL molar mass.

3.1.2. Analysis of the viscoelastic properties of PIL/IL solutions

The influence of the PIL molar mass on the viscoelastic properties of PIL/IL solutions at 10 wt. % in [C4mim][Cl] is illustrated in Fig. 3. At this PIL concentration, the three solutions and especially the one containing PIL_{100K} belong to the semi-dilute entangled regime, as $C \gg C^*$. It can be seen that PIL_{25K}/[C4mim][Cl] and PIL_{10K}/[C4mim][Cl] solutions exhibit a viscous modulus (G'') much higher than the storage modulus (G'), reflecting a fluid behavior. Furthermore, the G' values of PIL_{25K}/[C4mim][Cl], PIL_{10K}/[C4mim][Cl] and pure

[C4mim][Cl] exhibit a plateau at low frequency, which may indicate the presence of a weak network existing within the [C4mim][Cl] molecules. The properties of PIL_{10K}/[C4mim][Cl] are very close to the ones of pure [C4mim][Cl].

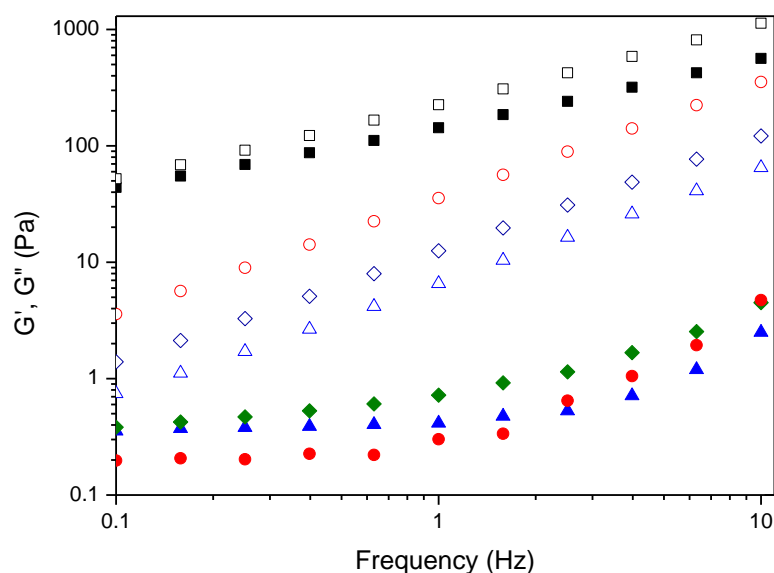


Fig. 3. Frequency-dependence of G' (filled symbols) and G'' (open symbols) moduli of PIL(10 wt%)/[C4mim][Cl] solutions, with 3 different molar masses: PIL_{10K} (◆), PIL_{25K} (●), PIL_{100K} (■) and pure [C4mim][Cl] (▲) at 25 °C.

The properties of PIL_{100K}/[C4mim][Cl] are quite different. This sample displays much larger G' and G'' moduli with a viscous dominant response, combined with a very low G'/G'' ratio on the entire frequency range, compared to the PIL(10wt%)/[C4mim][Cl] prepared with the lowest molar masses. After the introduction of PIL_{100K}, the plateau of G' is not visible anymore on the frequency range. For this mixture, the rheology response is mainly dictated by the PIL chains and the PIL/PIL entanglements. The observed enhancement of the viscoelastic properties is much probably caused by the formation of chain entanglements, which are more effective for PIL_{100K} /IL, since PIL_{100K} at 10 wt.% is well above C^* (actually in the semi-dilute entangled regime). In the remainder of this work, we will mainly focus on the use of PIL_{25K} and PIL_{100K}, since the behavior of PIL/[C4mim][Cl] systems with PIL_{25K} and PIL_{10K} is roughly the same.

3.1.3. Calculation of activation energies

The activation energies (E_a) were measured for PIL_{25K}/IL, PIL_{100K}/IL solutions, and compared to the ones of PIL/H₂O solutions and pure [C4mim][Cl] (Table 1). E_a can be seen as the barrier of energy to set in motion the species: IL and PIL chains, and thus the energy necessary to overcome intra- and intermolecular interactions. The E_a values were deduced either *i*) from the thermal-dependence of the Newtonian viscosity of solutions (in the 10-60 °C temperature range) for the fluid aqueous solutions (Fig. S8), or *ii*) from the thermal-dependence of viscoelastic moduli-frequency (over the 10-60 °C temperature range) for the more viscous PIL/IL solutions. In the second case, the G' and G'' moduli *versus* frequency were monitored at different temperatures, and the time-temperature superimposition principle was successfully applied to both G' , and G'' moduli. Master curves were obtained after the application of a horizontal shift a_t . The evolution of $\ln(a_t)$ as a function of the inverse of temperature is linear and obeys Arrhenius law, allowing for the determination of E_a (Fig. S9-S12). All the values are gathered in Table 1.

Table 1. Activation energies of various samples. For all samples $C_{PIL} = 10$ wt.%. * Determined from steady shear viscosity-temperature dependence, ** determined from time-temperature superimposition applied to G' , G'' -frequency dependence.

Samples	[C4mim][Cl] *	PIL _{10K} /H ₂ O*	PIL _{25K} /H ₂ O*	PIL _{100K} /H ₂ O *	PIL _{10K} /IL**	PIL _{25K} /IL**	PIL _{100K} / IL**
E_a (kJ/mol)	66	ND	11	12	72	78	81

From Table 1, different conclusions can be drawn. E_a values found for PIL /IL are particularly high (72, 78 and 81 kJ/mol), compared to the ones of the aqueous solutions, and are also superior to the one of pure [C4mim][Cl]. These values underpin *i*) the temperature-dependence of the interactions, and *ii*) the presence of strong polar interactions within PIL/IL solutions including hydrogen bonds and long-range electrostatic interactions between PIL and IL, and between IL molecules. These interactions contribute to enhance the cohesion of the

IL-based mixtures, in comparison with the aqueous ones. Again, these high E_a values emphasize the high propensity of [C4mim][Cl] to dissolve Poly([AEmim][Br]) chains. E_a increases with the molecular weight of the PIL and this is particularly pronounced in the case of PIL/IL solutions (72, 78, and 81 kJ/mol in IL against 11 and 12 kJ/mol in water). Increasing the PIL molar mass for $C = 10$ wt.% (superior to C^* , as found from concentration-viscosity dependence) tends to create additional chain entanglements leading to higher values of E_a

3.2. Thermal stability of PIL/IL binary blends

Thermogravimetric analysis was carried out to reveal the thermal stability of PIL/IL binary blends. The thermal degradation profiles of pure PILs of different molecular show an enhanced stability for the highest molar mass PIL (100 kg/mol). The thermal degradation temperatures $T_{d5\%}$ (considered as the temperature at which 5% of the material is decomposed) vary from 174 °C, to 202 °C and 240 °C, respectively (Fig. S4). Fig. 4, as a typical example, compares the thermal stability of [C4mim][Cl], PIL_{100K}, and PIL_{100K} (10 wt.%)/IL. The thermal decomposition profile of PIL/IL is intermediate between the behavior of PIL and the one of [C4mim][Cl]. The value of $T_{d5\%}$ of PIL_{100K} (10 wt.%)/IL binary blend (≈ 200 °C) is relatively close to the one of [C4mim][Cl], and lower than the value found for PIL_{100K} (240 °C). This intermediate thermal decomposition profile can be explained by the presence of physical interactions between PIL chains and IL molecules within the mixtures.

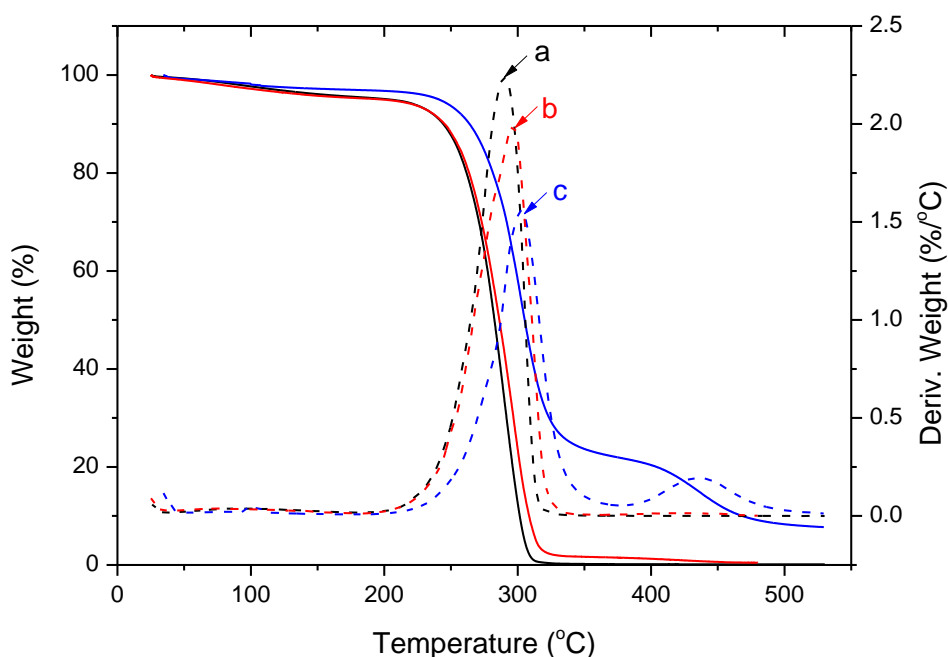


Fig. 4. TGA thermograms of of [C4mim][Cl] (a), PIL_{100K} (10 %)/ of [C4mim][Cl] (b) and PIL_{100K} (c).

3.3 Internal structure/organization of PIL/IL binary blends

X-ray scattering techniques such as WAXS and SAXS measurements were further conducted to obtain structural information on PIL/IL binary blends, at different length scales. Fig. 5 depicts the WAXS profiles of the binary blends of PIL_{25K} (10 wt.)/IL and PIL_{25K} (20 wt.)/IL in comparison to pure [C4mim][Cl] (previously molten and kept under a liquid at 25 °C). The WAXS pattern of pure [C4mim][Cl], displays an amorphous halo, characteristic of typical distances between neighboring molecules. No real diffraction peak could be identified in the pattern, proving the total disappearance of the initial crystallinity after the melting procedure. Moreover, such a short-chained imidazolium ionic liquid is a priori not expected to self-assemble into ordered micellar structures, as it can be observed for example for ionic liquids bearing long alkyl chains with 8 carbons or more [46-48]. In our case, the WAXS pattern of pure of [C4mim][Cl] solely shows a small shoulder at $q^* = 1.05 \text{ \AA}^{-1}$, which can be attributed to specific distances between anions [48-51].

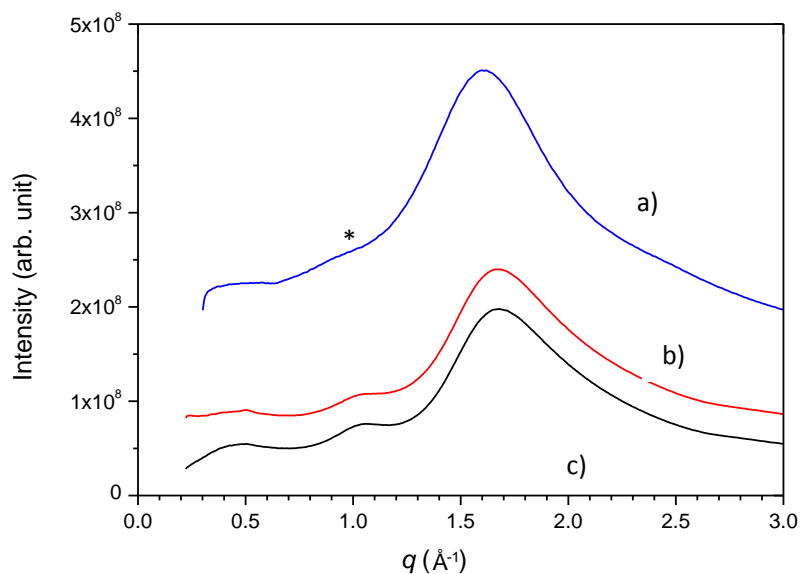


Fig. 5. WAXS pattern of [C4mim][Cl] (a), PIL_{25K} (10 wt.)/IL (b) and PIL_{25K} (20 wt.)/IL(c) at 25 °C.

To get deeper insight into the internal structure of the binary blends, SAXS measurements (I vs. q) were recorded on PIL_{25K}/IL at 10 and 20 wt.% (Fig. 6). For comparison, the SAXS pattern of the pure [C4mim][Cl] is included in Fig. 6.

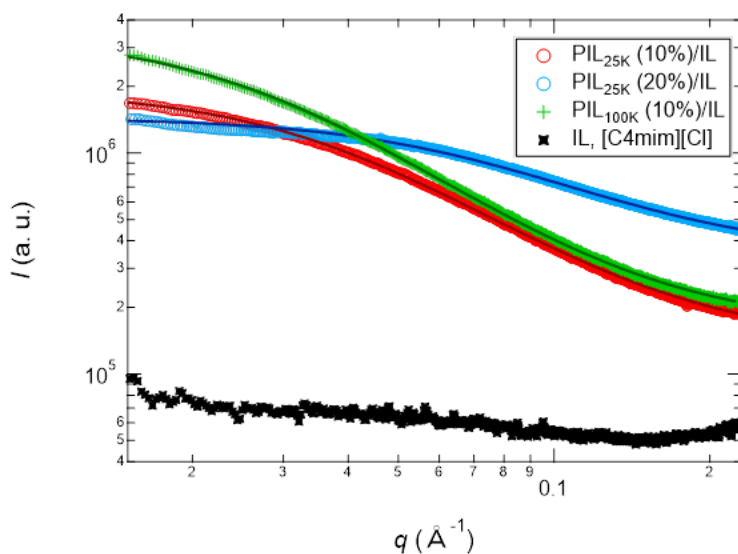


Fig. 6. SAXS pattern of [C4mim][Cl], PIL_{25K} (10 wt.)/IL, PIL_{25K} (20 wt.)/IL, and PIL_{100K} (10 wt.)/IL at 25°C

The scattering from the IL amorphous solvent is flat in the SAXS q -range [1.10^{-2} - $2.3 \cdot 10^{-1}$] \AA^{-1} . The scattering intensity of the PIL_{25K} /IL solutions is relatively weak due to the poor electronic contrast between PIL and IL, linked to their chemical similarity and possible ion exchanges between Br⁻ and Cl⁻. As the concentration of PIL solution reaches semi-dilute state ($C > C^*$), Lorentzian function was used to fit the SAXS data (eq. 1) [52-54]:

$$I(q) = I_0/(1+\zeta^2q^2) + I_{\text{sol}}, \quad (\text{eq. 1})$$

where ζ stands for the correlation length of concentration fluctuations and ($I_0 + I_{\text{sol}}$) stands for the scattered intensity extrapolated at $q = 0$.

The successful fittings of the scattering intensities using the Lorentzian model confirms the behavior of the PIL_{25k}/[C4mim][Cl] ($C = 10$ or 20 wt. %), as well as PIL_{100k}/[C4mim][Cl] ($C = 10$ wt.%) as semi-dilute polymer solutions with no aggregates or no “solid-like heterogeneities”. The correlation lengths ζ for PIL_{25K} (10%)/IL , PIL_{25K} (20%)/IL, and PIL_{100K} (100%)/IL are equal to 23.5, 13.4, and 35 \AA respectively. These characteristic distances should correspond to the thermal blob distance in semi-dilute solutions, following $\xi \propto \phi^{-3/4}$, and are naturally dependent on the PIL molar mass.

Additionally, Cryo-SEM experiments were achieved on a cross section of PIL_{100K} (10 wt.%)/IL binary blends, revealing a homogeneous structure with no segregated zones detected at the micrometric scale (Fig. 7). The high chemical affinity between PIL and IL molecules affords a completely compatible combination, resulting in uniform mixtures without microphase separation. Consistent with these results, EDX analysis (data not shown) recorded at different regions of the PIL_{100K} (10 wt.%)/IL sample indicated a homogeneous repartition of bromide, chloride, carbon, nitrogen and oxygen elements within all samples, which is also the result of ion exchange between bromide linked to the PIL and the chloride anion of [C4mim][Cl] .

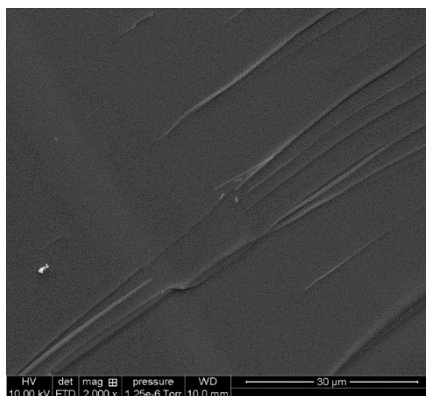


Fig. 7. Cryo-SEM images of a cross-section of PIL_{100K} (10 wt.)/IL binary blend.

3.4. Ionic transport properties

In order to underpin the effect of the addition of PIL on the ionic conductivity properties of [C4mim][Cl], the ionic transport properties were determined by broadband dielectric spectroscopy.

We exclusively analyzed the sample PIL_{100K} (10 wt.)/IL, since it corresponds to the system which exhibits the most interesting viscoelastic properties (see Fig. 3): G' is around 500 Pa at 10 Hz, and the gap between G' and G'' is very low. Given this combination ($C= 10$ wt.%, and $M = 100$ kg/mol) provides the sample the most adapted to potential applications (with enhanced G' and G'' moduli), its ionic conductivity was measured. The objective was to evaluate if the gain in viscoelasticity jeopardizes (or not) the ionic transport properties. Fig. S14 shows the frequency-dependence of the conductivity σ' ($\sigma' = \omega \varepsilon'' \varepsilon_0$, where ε_0 is the vacuum permittivity and ε'' is the dielectric loss) of the binary blend under isothermal conditions for temperatures ranging from 30 °C to -90 °C before thermal pretreatment. From Fig. S14, we can define the σ_{DC} value which corresponds to the value at the plateau. To limit the presence of water which favors ion dissociation and increase the ionic conductivity of electrolytes [55,56], a heat treatment (at 140 °C for 6 h) was applied to the hygroscopic PIL/IL solution. The resulting σ_{DC} of the PIL_{100K} (10 wt.)/IL solutions (before and after thermal treatment) was plotted as a function of the inverse temperature (Fig. 8).

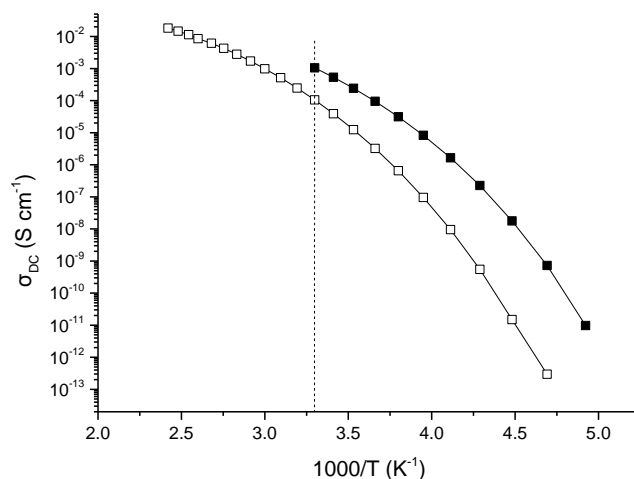


Fig. 8. Direct current conductivity (σ_{DC}) versus inverse temperature of PIL_{100K} (10 wt.)/IL before (filled symbols) and after thermal treatment (open symbols).

As classically observed, the σ_{DC} increases with temperature owing to the decrease of viscosity and the promotion of the overall mobility (PIL chains and IL molecules) [57]. Additionally, Fig. 8 shows that the temperature-dependence of conductivity exhibits the same convex upward curved profile over the entire temperature range, well modelled by the Voger-Fulcher-Tammann (VFT) equation: $\sigma_{DC} = \sigma_0 \exp(-B/(T-T_0))$, where σ_0 is the ionic conductivity at infinite temperature, B , a fitting parameter related to the activation energy of ion conduction, and T_0 , the Voger temperature linked to the ideal glass temperature [58-61]. Fig. 8 shows that, before the drying step, the PIL_{100K}(10 wt.)/IL binary blend exhibits high conductive properties with a σ_{DC} value of 1.0×10^{-3} S.cm⁻¹ at 30 °C. Under anhydrous conditions, the conductivity drops to *ca.* 1.0×10^{-4} S.cm⁻¹ at 30 °C, which is close to the conductivity of pure [C4mim][Cl] [62], remaining significantly high, in spite of the relatively high G' , and G'' moduli and high cohesion in the PIL/IL, as revealed by rheological investigation. Despite the establishment of multiple interactions between PIL and IL molecules, mobility is maintained at a level that promotes rapid ionic exchange and relatively high ionic conductivity, paving the way to the development and the design of functional materials with a promising potential as specific devices in the energy field [63]. The values obtained from the best fittings of the

experimental curves are given in Table S2. The B parameter, linked to the activation energy for ionic transport, is notably higher before the thermal treatment, possibly due to *i*) the plasticizer role of water which impacts the overall mobility of the system, and *ii*) the preferential affinities of ionic species for water which much probably enhances the ionic mobility.

4. Conclusion

In summary, we report a full investigation of never described solutions of poly([AEmim][Br]) in [C4mim][Cl]. The rheological properties of these solutions can be finely tuned by the concentration, the molecular weight of poly([AEmim][Br]), and the temperature. The influence of temperature allowed for calculating the activation energies of PIL/IL solutions which are particularly high (around 80 kJ/mol), compared to analogous PIL aqueous solutions (10 kJ/mol). This reflects a reinforced cohesion induced by multiple interactions between PIL chains and IL molecules, *i.e.* H-bonds and electrostatic interactions between the ionic species. A homogeneous morphology was evidenced at different length scales for all the PIL/IL solutions using WAXS, SAXS and SEM analyses. This is due to the good chemical compatibility between the components and to the ionic exchange between the bromide and chloride anions initially carried by PIL and IL respectively. PIL/IL mixtures with high PIL molar mass exhibit high conductivities (*ca.* 10^{-3} S/cm at 30 °C), in spite of the strong interactions established within the solutions. Poly([AEmim][Br])/ [C4mim][Cl] solutions synergize the advantageous features of both polyelectrolytes and ionic liquid molecules, which offers a large applicative potential notably in the field of energy devices.

5. Acknowledgements

B. Z. acknowledges the CSC program for a PhD grant. The authors gratefully acknowledge Pierre Alcouffe for SEM analyses and the “Centre Technologique des Microstructures de l'Université Claude Bernard Lyon1”.

Supporting Information. Complementary rheological, thermal, morphological analysis and conductive properties.

References

- [1]. Swatloski R. P., Spear S. K., Holbrey J. D., Rogers R. D., *J. Am. Chem. Soc.*, 2002, 124, 4974–4975.
- [2]. Schlufte K., Schmauder H.-P., Dorn S., Heinze T., *Macromol. Rapid Commun.*, 2006, 27, 1670–1676.
- [3]. Köhler S., Liebert T., Schöbitz M., Schaller J., Meister F., Gönther W., Heinze T., *Macromol. Rapid Commun.*, 2007, 28, 2311–2317.
- [4]. Pinkert A., Marsh K. N., Pang S., Staiger M. P., *Chem. Rev.*, 2009, 109, 6712–6728.
- [5]. Hayes R., Warr G. G., Atkin R., *Chem. Rev.*, 2015, 115, 6357–6426.
- [6]. Lei Z., Chen B., Koo Y.-M., MacFarlane D. R., *Chem. Rev.*, 2017, 117(10), 6633–6635.
- [7]. Yuan J., Mecerreyes D., Antonietti M., *Prog. Polym. Sci.*, 2013, 38, 1009–1036.
- [8]. Weber R. L., Ye Y., Schmitt A. L., Banik S. M., Elabd Y. A., Mahanthappa M. K., *Macromolecules*, 2011, 44, 5727–5735.
- [9]. Green M. D., Choi, J.-H., Winey, K. I., Long, T. E., *Macromolecules*, 2012, 45, 4749–4757.
- [10]. He H., Luebke D., Nulwala H., Matyjaszewski M., *Macromolecules*, 2014, 47, 6601–6609.
- [11]. Vijayakrishna K., Jewrajka S. K., Ruiz A., Marcilla R., Pomposo J. A., Mecerreyes D., Taton D., Gnanou Y., *Macromolecules*, 2008, 41, 6299–6308.
- [12]. Depoorter J., Yan X., Zhang B., Sudre G., Charlot A., Fleury E., Bernard J., 2021, *Polym. Chem.*, 12(1), 82–91.
- [13]. Srour H., Leocmach M., Maffei V., Ghogia A. C., S Denis-Quanquin., Taberlet N., Manneville S., Andraud C., Bucher C., Monneréau C., *Polym. Chem.*, 2016, 7, 6608–6616.
- [14]. Qian W., Texter J., Yan F., *Chem. Soc. Rev.*, 2017, 46(4), 1124–1159.
- [15]. Cordella D., Kermagoret A., Debuigne A., Jérôme C., Mecerreyes D., Isik M., Taton D., Detrembleur C., *Macromolecules*, 2015, 48, 5230–5243.
- [16]. Aqil M., Aqil A., Ouhib F., Idrissi A. E., Dahbi M., Detrembleur C., Jérôme C., *Eur. Polym. J.*, 2021, 152, 110453.
- [17]. Mecerreyes D., *Prog. Polym. Sci.*, 2011, 36, 1629–1648.
- [18]. Cowan M. G., Lopez A. M., Masuda M., Kohno Y., McDanel W. M., Noble R. D., Gin D. L., *Macromol. Rapid Commun.*, 2016, 37, 1150–1154.
- [19]. Wang P. H., Wang T. L., Lin W. C., Lin H. Y., Lee M. H., Yang C. H., *Nanomaterials*, 2018, 8, 225.
- [20]. De Oliveira P. S. C., Alexandre S. A., Silva G. G., Trigueiro J. P. C., Lavall R. L., *Eur. Polym. J.*, 2018, 108, 452–460.
- [21]. Zhao J., Shen X., Yan F., Qiu L., Lee S., Sun B., *J. Mater. Chem.*, 2011, 21, 7326–7330.
- [22]. Zhang S.-Y., Zhuang Q., Zhang M., Wang H., Gao Z., Sun J.-K., Yuan J., *Chem. Soc. Rev.*, 2020, 49, 1726–1755.
- [23]. Cowan M. G., Gin D. L., Noble R. D., *Acc. Chem. Res.*, 2016, 49, 724–732.
- [24]. Gin D. L., Noble R. D., *Science*, 2011, 332, 674–676.
- [25]. Dai Z., Noble R. D., Gin D. L., Zhang X., Deng L., *J. Membr. Sci.*, 2016, 497, 1–20.
- [26]. Tomé L. C., Marrucho I. M., *Chem. Soc. Rev.*, 2016, 45, 2785–2824.
- [27]. Tomé L. C., Mecerreyes D., Freire C. S. R., Rebel L. P. N., Marrucho I. M., *J. Membr. Sci.*, 2013, 428, 260–266.
- [28]. Bara J. E., Hatakeyama E. S., Gin D. L., Noble R. D., *Polym. Adv. Technol.*, 2008, 19, 1415–1420.
- [29]. Carlisle T. K., Nicodemus G. D., Gin D. L., Noble R. D., *J. Membr. Sci.*, 2012, 397–398, 24–37.
- [30]. Shaligram S. V., Wadgaonkar P. P., Kharul U. K., *J. Membr. Sci.*, 2015, 493, 403–413.
- [31]. Gouveia A. S. L., Ventaja L., Tomé L. C., Marrucho I. M., *Membranes*, 2018, 8, 124.
- [32]. Sappidi P., Liu X., O’Harra K. E., Bara J. E., Turner C. H., *Macromolecules*, 2021, 54, 1611–162.
- [33]. Zhang B., Yan X., Alcouffe P., Charlot A., Fleury E., and Bernard J., *ACS Macro Lett.*, 2015, 4, 1008–1011.
- [34]. Zhang B., Sudre G., Quintard G., Serghei A., David L., Bernard J., Fleury E., Charlot A., *Carbohydr. Polym.*, 2017, 157, 586–595.

- [35]. Gericke M., Schluffer K., Liebert T., Heinze T., Budtova T., *Biomacromolecules*, 2009, 10, 1188–1194.
- [36]. Kuang Q.-L., Zhao J.-C., Niu Y.-H., Zhang J., Wang Z.-G., *J. Phys. Chem. B*, 2008, 112, 10234–10240.
- [37]. Sescousse R., Le K. A., Ries M. E., Budtova T., *J. Phys. Chem. B*, 2010, 114, 7222–7228.
- [38]. Sangoro J. R., Iacob C., Serghei A., Friedrich C., Kremer F., *Phys. Chem. Chem. Phys.*, 2009, 11, 913–916.
- [39]. Serghei A., Tress M., Kremer F., *Phys. Rev. B*, 2009, 80, 184301.
- [40]. Regalado E. J., Selb J., Candau F., *Macromolecules*, 1999, 32, 8580-8588.
- [41]. Tam K. C., Tiu C., *J. Rheol.*, 1989, 33, 257-280.
- [42]. Dobrynin A. V., Colby R. H., Rubinstein M., *Macromolecules*, 1995, 28, 1859-1871.
- [43]. DeGennes P. G., *Scaling Concepts in Polymer Physics*, Cornell University Press : Thaca, New York., 1979.
- [44]. Doi M., Edwards S. F., *The theory of polymer dynamics*, Claderon Press: Oxford, England, 1986.
- [45]. Swatloski R. P., Spear S. K., Holbrey J. D., Rogers R. D., *J. Am. Chem. Soc.*, 2002, 124, 4974-4975.
- [46]. Bradley A. E., Hardacre C., Holbrey J. D., Johnston S., McMath S. E. J., Nieuwenhuyzen M., *Chem. Mater.*, 2002, 14, 629-635.
- [47]. Katayanagi H., Hayashi S., Hamaguchi H., Nishikawa K., *Chem. Phys. Lett.*, 2004, 392, 460-464.
- [48]. Triolo A., Russina O., Bleif H.-J., Di Cola E., *J. Phys. Chem. B*, 2007, 111, 4641-4644.
- [49]. Saha S., Hayashi S., Kobayashi A., Hamaguchi H., *Chem. Lett.*, 2003, 32,740-741.
- [50]. Hayes R., Warr G. G., Atkin R., *Chem. Rev.*, 2015, 115, 6357-6426.
- [51]. Greaves T. L., Kennedy D. F., Mudie S. T., Drummond C. J., *J. Phys. Chem. B*, 2010, 114, 10022-10031.
- [52]. Hamada F., Kinugasa S., Hayashi H., Nakajima A., *Macromolecules*, 1985, 18, 2290-2294.
- [53]. Saito S., Hashimoto T., Morfin I., Lindner P., Boue F., *Macromolecules*, 2002, 35, 445-459.
- [54]. Vidinha P., Lourenco N. M. T., Pinheiro C., Bras A. R., Carvalho T., Santos-Silva T., Mukhopadhyay A., Romao M. J., Parola J., Dionisio M., Cabral J. M. S., Afonso C. A. M., Barreiros S., *Chem. Commun.*, 2008, 5842-5844.
- [55]. Akgol Y., Hofmann C., Karatas Y., Cramer C., Wiemhofer H. D., Schonhoff M., *J. Phys. Chem. B*, 2007, 111, 8532–8539.
- [56]. Spohr H. V., Patey G. N., *J. Chem. Phys.*, 2010, 132, 234510.
- [57]. Sood R., Zhang B., Serghei A., Bernard J., Drockenmuller E., (2015). *Polym. Chem.*, 2015, 6, 3521–3528.
- [58]. Buchtová N., Guyomard-Lack A., Le Bideau J., *Green Chem.*, 2014, 16, 1149–1152.
- [59]. Dias A. M. A., Cortez A. R., Barsan M. M., Santos J. B., Brett C. M. A., De Sousa H.C., *ACS Sustain Chem. Eng.*, 2013, 1, 1480–1492.
- [60]. Trivedi T. J., Srivastava D. N., Rogers R. D., Kumar A., *Green Chem.*, 2012, 14, 2831–2839.
- [61]. Vidinha P., Lourenço N. M. T., Pinheiro C., Brás A. R., Varvalho T., Santos-Silva T., Mukhopadhyay A., Romao M. J., Parola J., Dionisio M., Cabral J. M. S., Afonso C. A. M., Barreiros S., *Chem. Commun.*, 2008, 44, 5842–5844.
- [62]. Depoorter J., Mourlevat A., Sudre G., Morfin I., Prasad K., Serghei A., Bernard J., Fleury E., Charlot A., *ACS Sustain. Chem. Eng.*, 2019, 7, 16747-16756.
- [63]. Yang B., Yang G., Zhang Y.-M., Zhang S. X.-A., *J. Mater. Chem. C*, 2021, 9, 4730-4741.